Acta Crystallographica Section D
Biological Crystallography
ISSN 0907-4449

An engineered PII protein variant that senses a novel ligand: atomic resolution structure of the complex with citrate

Kornelius Zeth,[a]*‡ Oleksandra Fokina[b] and Karl Forchhammer[b]*

[a]Department of Protein Evolution, Max Planck Institute for Developmental Biology, Spemannstrasse 35, 72076 Tübingen, Germany, and [b]Interfakultäres Institut für Mikrobiologie und Infektionsmedizin der Eberhard-Karls-Universität Tübingen, Auf der Morgenstelle 28, 72076 Tübingen, Germany

‡ Current address: ZMBP, University of Tübingen, Auf der Morgenstelle 1, 72076 Tübingen, Germany.

Correspondence e-mail: kornelius.zeth@googlemail.com, karl.forchhammer@uni-tuebingen.de

Received 26 January 2012
Accepted 16 April 2012

PDB Reference: PII-I86N, complex with ATP, magnesium and citrate, 4aff.

PII proteins are central signal processing units for the regulation of nitrogen metabolism in bacteria, archaea and plants. They act in response to cellular energy, carbon and nitrogen availability. The central metabolites ATP, ADP and 2-oxoglutarate, which indicate cellular energy and carbon/nitrogen abundance, bind in a highly organized manner to PII and induce effector-molecule-dependent conformational states of the T-loop. Depending on these states, PII proteins bind and modulate the activity of various regulatory targets. A mutant variant of the *Synechococcus elongatus* PII protein (PII-I86N) has been identified to have impaired 2-oxoglutarate binding. Here, the PII-I86N variant was cocrystallized in the presence of ATP, magnesium and citrate and its structure was solved at a resolution of 1.05 Å. The PII-I86N variant bound citrate in place of 2-oxoglutarate. Citrate binding is mediated primarily by interactions with the ATP-coordinated magnesium ion and the backbone atoms of the T-loop. Citrate binding rearranges the conformation of the T-loop and, consistent with this, citrate suppresses the binding of PII-I86N to an NAG kinase variant, which is similar to the suppression of PII–NAG kinase complex formation by 2-OG. Based on the structures of 2-OG and citrate, homocitrate was suggested as a third ligand and an efficient response towards this molecule with different functional properties was observed. Together, these data provide a first glimpse of a genetically engineered PII variant that senses a new effector molecule.

1. Introduction

PII proteins are abundant and highly conserved signal integrators in bacteria, archaea and plants. They act as signal-processing units for the regulation of nitrogen metabolism in response to cellular energy, carbon and nitrogen availability, which is interpreted through the binding of the central metabolites ATP, ADP and 2-oxoglutarate (2-OG; Forchhammer, 2008; Leigh & Dodsworth, 2007; Ninfa & Jiang, 2005; Sant'Anna *et al.*, 2009). All PII proteins follow the same architectural principles and have highly conserved three-dimensional structures. The subunits are 12–13 kDa polypeptides comprising an α/β protein fold, which assemble to form a small cylindrical homotrimer (Figs. 1*a* and 1*b*; Sakai *et al.*, 2005; Xu *et al.*, 1998, 2003). The central core of the trimer formed by β-sheets is surrounded by α-helices (Figs. 1*a* and 1*b*). Furthermore, each subunit exposes three peripheral loops, which are positioned in the clefts between the subunits. The large solvent-exposed and flexible T-loop projects outside the intersubunit cleft, connecting the β2 and β3 sheets. Two

smaller rigid loops, the B-loop and C-loop, from opposite subunits face each other in the intersubunit cleft. The basis of the T-loop as well as the B-loop and C-loop essentially constitutes the binding site for the effector molecules and these cleft regions can thus be regarded as the binding sites of the signal processor PII. ATP is efficiently coordinated by an array of positively charged residues, mostly from the C-loop and the B-loop (Xu *et al.*, 1998, 2001; Fig. 1*a*). ADP competes with ATP for the binding sites (Fokina *et al.*, 2011; Jiang & Ninfa, 2007).

The mode of 2-OG binding has recently been explored by crystallographic analysis of the *Synechococcus elongatus* PII protein (PDB entries 2xul and 2xun; Fokina, Chellamuthu, Forchhammer *et al.*, 2010), a model for cyanobacterial and plant PII proteins, as well as of the PII proteins GlnZ from the proteobacterium *Azospirillum brasiliense* (PDB entry 3myh; Truan *et al.*, 2010) and GlnK3 from the thermophilic archaeon *Archaeoglobus fulgidus* (PDB entry 3ta2; Maier *et al.*, 2011). In all cases, binding of 2-OG is mediated by a bridging Mg^{2+} ion, which has sixfold coordination involving oxo groups of all three phosphates of ATP, the α-carboxy O atom and the keto O atom of 2-OG and the amido O atom of residue 39, which completes the octahedral coordination. Further contribution to 2-OG binding is provided by a salt bridge formed between the γ-carboxy O atoms of 2-OG and Lys58 and by hydrogen-bonding interactions between 2-OG and the backbone of the basal part of the T-loop (residues 39–41). Binding of 2-OG results in an extended structural rearrangement of the T-loop, which is the key process in regulation of most PII interactions (Forchhammer, 2008). The PII targets in cyanobacteria are *N*-acetylglutamate kinase (NAGK), which catalyses the

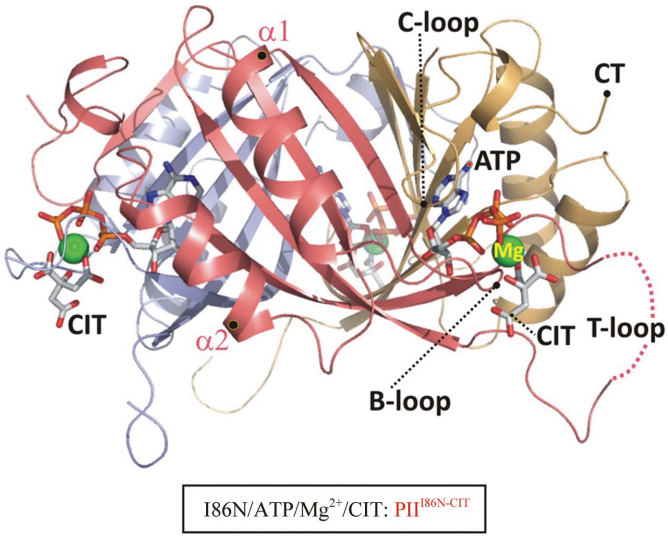

(*a*)

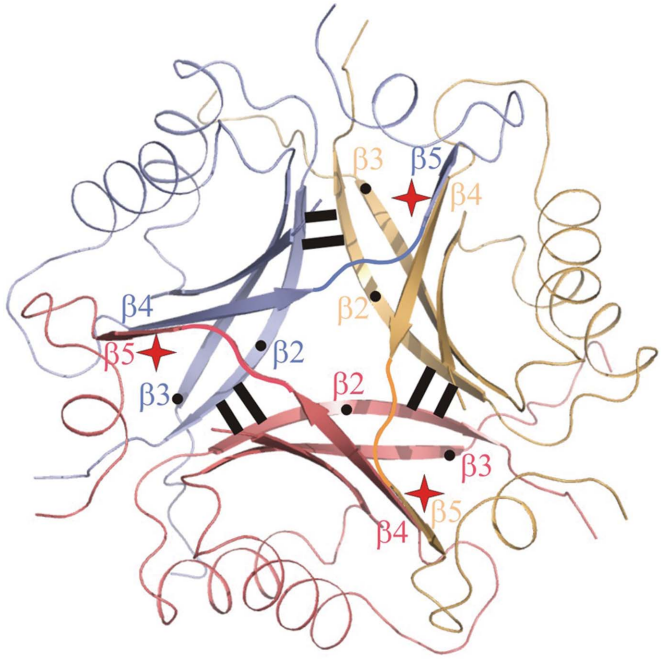

(*b*)

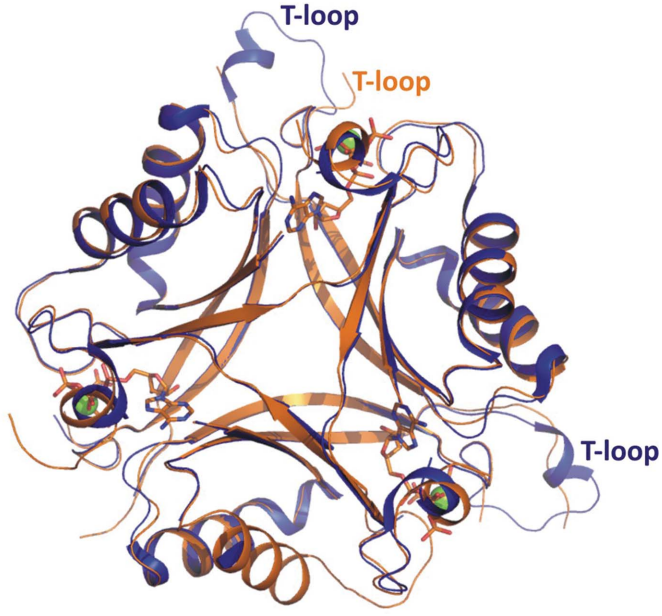

(*c*)

Figure 1
The trimeric structure and core stability of the I86N mutant PII protein from *S. elongatus*. (*a*) Side view of the trimeric $PII^{I86N\text{-}CIT}$ mutant protein complex in cartoon representation. The three individual subunits are coloured light blue, light red and light orange. Loop elements known to be archetypal of the large class of PII proteins (the B-loop, C-loop and T-loop) are indicated. The unstructured T-loop of this structure is marked in dashed lines. The two ligands ATP and citrate (CIT) are highlighted in stick representation and the magnesium ion (Mg) is shown as a green sphere. (*b*) Top view onto the trimeric complex with the same colour scheme as in (*a*). The β-sheet core of the protein is highlighted and important secondary-structure elements are marked. The formation of intermolecular β-twist structures through hydrogen-bond networks between three β2 strands is indicated by black lines. The three-dimensional domain swap of β5 upon antiparallel pairing with β4 of the neighbouring subunit is indicated by stars. (*c*) The same top view of two trimeric 2-OG-bound structures using wild-type PII proteins from *S. elongatus* and *A. brasiliense* with ATP, Mg and 2-OG (PDB entry 3mhy, GlnZ, dark blue; PDB entry 2xul, PII^{OGex}, orange). The two structures are virtually identical, with an r.m.s.d. of 0.62 Å for 103 aligned C^{α} atoms. In the GlnZ structure two of the T-loops of the trimeric protein are visibly ordered, while in the PII wild-type structure from *S. elongatus* PII^{OGex} none of these loops are ordered.

committed step in arginine biosynthesis (Burillo *et al.*, 2004; Heinrich *et al.*, 2004; Maheswaran *et al.*, 2004), and PipX, a transcriptional co-activator of the major N-control transcription factor NtcA in cyanobacteria (Espinosa *et al.*, 2006, 2007). The structures of cyanobacterial NAGK and PipX proteins in complex with PII have been resolved (Llácer *et al.*, 2007, 2010). These structures clearly revealed that the T-loop in the 2-OG-bound state is incompatible with receptor-complex formation (Fokina, Chellamuthu, Forchhammer *et al.*, 2010).

An important aspect in the signal-processing function of PII proteins is the mutual influence of the three active sites on each other. The mode of cooperativity may differ between PII proteins. *S. elongatus* PII displays negative cooperativity during the occupation of the three sites by ATP, ADP and 2-OG (Fokina, Chellamuthu, Zeth *et al.*, 2010; Forchhammer & Hedler, 1997), whereas the PII protein GlnB from *Escherichia coli* shows anti-cooperativity for ATP and 2-OG binding but not for ADP binding (Jiang & Ninfa, 2007). The *A. fulgidus* GlnK3 protein shows strong negative cooperativity for 2-OG binding but not for ATP binding (Maier *et al.*, 2011). In previous work, we determined the structure of an *S. elongatus* PII crystal containing PII trimers with all three sites occupied by ATP but containing one, two or three bound 2-OG molecules (Fokina, Chellamuthu, Forchhammer *et al.*, 2010). This structure provided the first insights into the mechanism of intersubunit signalling by showing that the binding of one 2-OG molecule differentially affects the ATP structure in the second and third binding sites.

In an attempt to gain further insight into the function of PII signal processing in *S. elongatus*, mutants of PII were generated by random mutagenesis and screened for altered interaction with NAGK, which is the major receptor protein of cyanobacterial PII proteins. Two variants were discovered (replacement of Ile86 by Asn or Thr; I86N and I86T) which displayed 2-OG-insensitive NAGK binding (Fokina, Chellamuthu, Zeth *et al.*, 2010). The structure of PII-I86N in complex with ATP was solved, showing that the Ile86-to-Asn replacement resulted in a T-loop conformation which mimicked the NAGK-bound state. The insensitivity towards 2-OG resulted from the closure of the 2-OG binding site owing to a new hydrogen-bonding interaction between Asn86 and the backbone O atom of Thr43, which leads to Lys58–Glu44 salt-bridge formation accompanied by tight folding of the T-loop (Fokina, Chellamuthu, Zeth *et al.*, 2010). Thus, the mutation of a B-loop residue impairs the binding of 2-OG in an indirect manner and shows that the binding properties of PII proteins can be manipulated by distant amino-acid replacements.

In this study, we show that the I86N PII variant binds citrate instead of 2-oxoglutarate, providing the first example of a genetically engineered PII protein that senses a novel effector molecule. The structural data, together with supporting biochemical data, provide insight into the binding mechanism of citrate and the suppression of complex formation with the NAGK enzyme, in analogy to the activity of 2-OG. Furthermore, this mutant structure extends the unusual plasticity of the PII protein family and exemplifies a route to the generation of novel sensor proteins for novel molecules.

2. Materials and methods

2.1. Overexpression and purification of recombinant *S. elongatus* PII and NAGK

The wild-type and the I86N mutant *glnB* genes cloned into the Strep-Tag fusion vector pASK-IBA3 (IBA, Göttingen, Germany) were overexpressed in *E. coli* RB9060 (Bueno *et al.*, 1985) and purified using affinity chromatography as described previously (Heinrich *et al.*, 2004). His-tagged recombinant wild-type NAGK and the R233A variant were overexpressed in *E. coli* BL21 (DE3) (Studier *et al.*, 1990) and purified as described previously (Maheswaran *et al.*, 2004).

2.2. Surface plasmon resonance detection (SPR)

SPR experiments were performed using a BIAcore X biosensor system (Biacore AB, Uppsala, Sweden) at 298 K in HBS-Mg buffer consisting of 10 m*M* HEPES pH 7.5, 150 m*M* NaCl and 0.005% Nonidet P-40 at a flow rate of 15 µl min^{-1} as described previously (Maheswaran *et al.*, 2004). The purified His_6-NAGK was immobilized on the Ni^{+}-loaded NTA sensor chip in flow cell 2 (FC2) in a volume of 50 µl at a concentration of 30 n*M* (hexamer) to receive a binding signal of approximately 3000 resonance units (RU), which corresponds to a surface concentration change of 3 ng mm^{-2}. For measurement of the inhibition of the wild-type PII–NAGK interaction by 2-OG or the inhibition of the I86N and R233A PII–NAGK interactions by citrate/homocitrate, the PII protein was diluted in HBS buffer with 1 m*M* $MgCl_2$, 1 m*M* ATP and different concentrations of 2-OG or citrate and then injected into both FC1 and FC2 with bound His_6-NAGK. The specific binding of PII to NAGK and the dissociation was recorded as the response signal difference FC2 − FC1. PII was removed from the His_6-NAGK surface by injecting 25 µl 1 m*M* ADP. To reload the proteins onto the NTA sensor chip, 25 µl 0.4 *M* EDTA pH 7.5 was injected to remove the His_6-NAGK and Ni^{2+}. Subsequently, the chip could be loaded again with 5 m*M* Ni_2SO_4 solution and His_6-NAGK as described above.

2.3. Crystallization of recombinant *S. elongatus* PII protein mutant

Crystallization was performed by the sitting-drop technique by mixing 400 nl protein solution with an equal amount of reservoir solution using a Honeybee robot (Genomic Solutions Ltd). Drops were incubated at 293 K and images were recorded using a RockImager system (Formulatrix, Waltham, Massachusetts, USA). The buffer for PII-I86N was composed of 10 m*M* Tris pH 7.4, 0.5 m*M* EDTA, 100 m*M* NaCl, 1% glycerol, 2 m*M* ATP-Mg and crystals appeared after 7 d in a precipitant condition consisting of 0.1 *M* trisodium citrate dihydrate pH 5.6, 20% polyethylene glycol (PEG) 4000 and 0.2 *M* ammonium acetate. Crystals were mounted directly in cryoloops and flash-cooled in liquid nitrogen. Glycerol was used as the cryoprotectant. Diffraction data were collected at the Swiss Light Source (SLS; Villigen, Switzerland). Diffraction images were recorded on a MAR CCD 225 plate (MAR Research, Norderstedt, Germany) and were processed using

XDS/*XSCALE* (Kabsch, 2010). The structure was solved by molecular replacement using *MOLREP* (Vagin & Teplyakov, 2010) with the PII-I86N structure (PDB entry 2xbp; Fokina, Chellamuthu, Zeth *et al.*, 2010) as a search model. Rebuilding of the structure and refinement was performed using *Coot* and *REFMAC* (Emsley & Cowtan, 2004; Murshudov *et al.*, 2011). The quality of the structure was analyzed using *PROCHECK* (Laskowski *et al.*, 1993). All crystallographic figures were generated using the graphical interface of *PyMOL* (http://www.pymol.org).

Table 1
Data-collection and refinement statistics for $PII^{I86N\text{-}CIT}$.

Values in parentheses are for the highest resolution shell.

Data collection	
Space group	$P6_3$
Unit-cell parameters	
$a = b$ (Å)	62.09
c (Å)	51.17
$\alpha = \beta$ (°)	90
γ (°)	120
Resolution (Å)	37–1.05 (1.11–1.05)
R_{merge}	0.09 (0.74)
$\langle I/\sigma(I)\rangle$	12.2 (2.1)
Completeness (%)	99.6 (98.3)
Multiplicity	7.2 (6.5)
Refinement	
Resolution (Å)	37–1.05 (1.07–1.05)
No. of reflections	49584 (2611)
R_{work}/R_{free}	0.12/0.14 (0.24/0.25)
Total No. of atoms	1039
Protein (chains/residues)	1/107
Ligands (ATP/citrate/Mg^{2+})	1/1/1
Water	130
B factors (Å^2)	
Protein	6.3
Ligand/ion (ATP/citrate/Mg^{2+})	5.7/8.6/6.1
Water	20.2
R.m.s. deviations	
Bond lengths (Å)	0.030
Bond angles (°)	2.5
PDB code	4aff

3. Results and discussion

3.1. Architecture of PII proteins as a prerequisite for ligand binding

All PII proteins follow the same architectural principle: they are small signalling proteins (3.5 × 5.5 nm) comprising an α/β protein fold. Fig. 1 shows a cartoon representation of PII-I86N ($PII^{I86N\text{-}CIT}$) from *S. elongatus*. The trimerization and three-dimensional domain swapping of the C-terminal β5 sheet with the β4 strand of the subunit located clockwise resembles the quarternary structure of all PII proteins (Cheah *et al.*, 1994; Leigh & Dodsworth, 2007; Forchhammer, 2008). The three subunits form an extended and intertwined triangular β-core structure surrounded by six elongated α-helices (Figs. 1*a* and 1*b*). The central core of the complex is formed by three extended β2 strands which pair with the neighbouring $\beta2'$ and $\beta2''$ strands, respectively (Fig. 1*b*). Two subunits form the ligand binding site for ATP/ADP essentially through the positively charged residues Arg38 (ATP: O1B, O3G), Lys90 (ATP: O2B) and the Gly89 backbone atoms from one subunit and Arg101′ (ATP: O2B, O3B) and Arg 103′ (ATP: O2G, O3G) from the adjacent subunit. Furthermore, the adjacent subunit contributes to interactions with the adenine moiety, most importantly Thr29 (Fig. 2). Lys90 residue connects to both, the β-phosphate and the imido nitrogen of the adenine base to influence the relative conformation of these substructures by contacts. This tight coordination of ATP is a prerequisite for Mg^{2+} stabilization and provides the structural

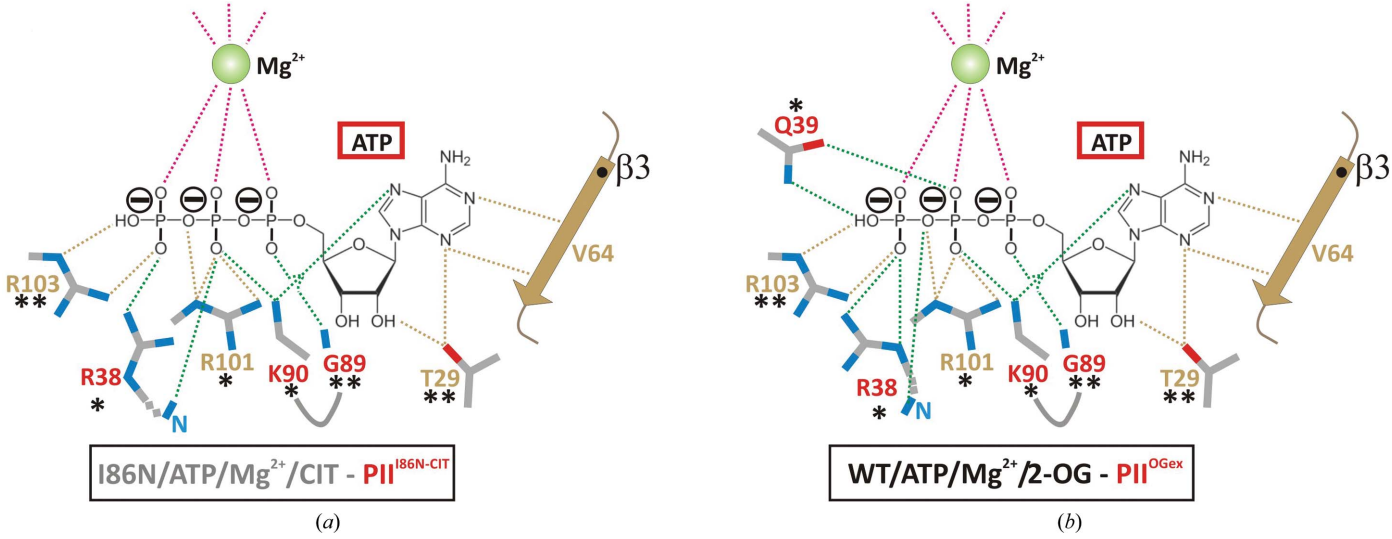

Figure 2
Binding-mode comparison of ATP in the mutant and wild-type structures. (*a*) Detailed schematic view of the ATP-binding site of $PII^{I86N\text{-}CIT}$. The residues from two PII subunits (residues are colour-coded in red and gold) that coordinate the binding site are shown in stick representation and the residue numbers are shown in corresponding colours. The conservation of these residues is indicated by * (strongly conserved) and ** (completely conserved). (*b*) Binding mode of ATP in the wild-type structure.

architecture for the sensory mechanism towards 2-OG, which is followed by control or signal integration into the cascades of various cellular networks, respectively.

In previous work, we have determined the structure of wild-type PII from *S. elongatus* and have identified complexes of the protein with one, two and three 2-OG molecules bound (excess 2-OG, PII^{OGex}, PDB entry 2xul; low 2-OG, PII^{OG1-3}, PDB entry 2xun; Fokina, Chellamuthu, Forchhammer *et al.*, 2010). Three other structures of PII-family members bound to 2-OG signalling molecules have been reported: GlnK1 (PDB entry 2j9d) from *Methanococcus jannaschii* (Yidiz *et al.*, 2007), GlnZ (PDB entry 3mhy; only two of the three T-loops are ordered) from *A. brasiliense* (Truan *et al.*, 2010) and GlnK3 (PDB entry 3ta2) from *A. fulgidus* (Maier *et al.*, 2011). The *M. jannaschii* structure shows significantly different locations of the ligand and presumably represents a crystallization artifact. In contrast, the binding of 2-OG through ligation of Mg^{2+} is essentially identical in the PII structures from *S. elongatus*, *A. brasiliense* and *A. fulgidus* (Fig. 1*c*). Notably, the structures of the *S. elongatus* PII–ATP–2-OG complex (PII^{OGex}) and of *A. brasiliense* GlnZ and *A. fulgidus* GlnK3 complexed with ATP and 2-OG show the entire T-loop in an ordered conformation, whereas in the PII^{OGex} structure its distal part is largely disordered (Fig. 1*c*). However, the T-loops in the GlnZ structure form tight crystal contacts with neighbouring trimers similar, for example, to the structure of *S. elongatus* PII in the absence of cofactors (Xu *et al.*, 2003); consequently, the stabilization of the T-loop in one conformation may not resemble the ensemble in solution. Therefore, it remains possible that the distal part of the T-loop of single PII molecules complexed with effector molecules is indeed flexible in solution. In contrast, the basal part of the T-loop is fixed in defined positions in response to binding of the effector molecules. The strongly structured ATP-binding site, which is a structural prerequisite for Mg^{2+} binding followed by ligand interaction and reorientation of the protein periphery, is conserved in almost all PII proteins analyzed to date and is schematically shown in Fig. 2(*b*).

Previously, the structure of an I86N mutant of *S. elongatus* PII which was insensitive towards 2-OG was determined in complex with ATP and Mg^{2+}. In this structure, the T-loop is locked in a tightly folded conformation by Asn86, which hydrogen bonds to the T-loop backbone residue Thr43 at the outer surface of the PII protein, while the Glu44 residue forms a salt bridge to Lys58 to further stabilize the downwards bent conformation of the extended loop structure (see Fig. 3*a*). Furthermore, the loop architecture is strongly bent by the interaction with Mg^{2+} through the carbonyl group of Gly37. Additional residues of minor importance are marked in Fig. 3(*a*). The inability of this mutant to bind 2-OG may be

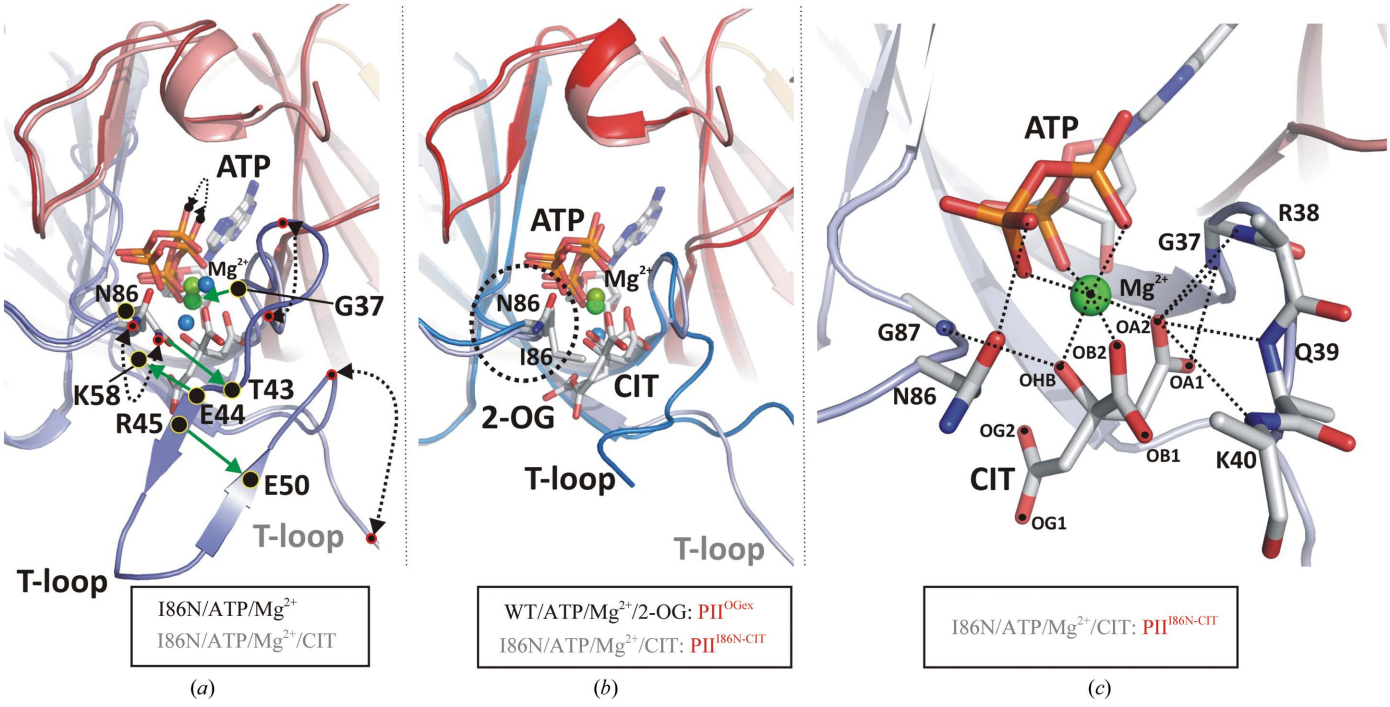

Figure 3
Plasticity of the cofactor-binding site in the $PII^{I86N-CIT}$ structure. (*a*) Close up of a superposition of two I86N mutant structures crystallized in the presence and absence of citrate ligands. Significant changes upon binding of the citrate cofactor are marked by dashed lines and arrows. These changes are particularly strong in the conformation of ATP and the Asn86 side chain, and subsequently in the T-loop stabilization. The residues that are important in stabilizing the T-loop interactions in the I86N mutant are marked by circles and interactions are indicated by green arrows. (*b*) Close up of a superposition of PII^{OGex} and $PII^{I86N-CIT}$ structures with the important features of the active site highlighted. The two structures superpose well, although the active sites have a different stereochemistry. (*c*) Structural basis of citrate binding in $PII^{I86N-CIT}$. Two modes of interactions are important: interactions with the Mg ion coordinated by ATP and the hydrogen bonds to the backbone atoms of residues located on the T-loop. Residues in the proximity of the citrate molecule are marked by dashed lines.

explained by the strongly locked interface, which results in a strongly reduced affinity for 2-OG. This structure essentially resembles the conformation originally obtained in a PII–NAGK complex in the absence of ATP and additional ligands. As a consequence of this similarity, the I86N variant is a superactive NAGK binder and NAGK complex formation is not impaired by 2-OG (Fokina, Chellamuthu, Zeth *et al.*, 2010).

3.2. Plasticity of the PII binding site

The complex of the I86N mutant protein with Mg-ATP and another physiologically relevant molecule, citrate, yielded crystals that diffracted to atomic resolution with a monomer in the asymmetric unit (see Table 1 for crystallographic statistics). The overall structures in the presence and absence of citrate are virtually identical, with the only significant difference being that the binding of citrate leads to disorder of the bent T-loop conformation (see Fig. 3*a*). Structure superposition of $PII^{I86N\text{-}CIT}$ and PII^{OGex} indicates the structures to be virtually identical except in the conformations of the T-loop structures (see Fig. 3*b*). Citrate is bound at a similar position to 2-OG in the wild-type structure (Fig. 3*b*). O atoms OA2, OB2 and OH2 of citrate form the second half of the ligation sphere of the Mg^{2+} ion. Additional hydrogen bonds are formed, in particular from OA2 to the backbone N atoms of Gly37, Arg38, Gln39 and Lys40, from OHB to Gly87 and from OA1 to Gly37 (Fig. 3*c*). In contrast to 2-OG, citrate does not form any interactions with side-chain residues and therefore appears to be largely independent of coordination to potentially conserved residues (see Figs. 3*b* and 4*d*).

Citrate induced disorder in the T-loop conformation that closely resembled that of wild-type PII complexed with Mg-ATP and 2-OG (see Fig. 3*b*). The citrate molecule breaks the Asn86–Thr43 hydrogen bond, which locks the 2-OG binding site. Citrate thus causes reorientation of the Asn86 side chain, with release of the T-loop into a loosened conformation. The energy gained by coordination of the Mg^{2+} ion is possibly one of the major driving forces for citrate binding (see the schematic representations of the Mg^{2+} environment in the three structures in Figs. 4*a*–4*c*). The ATP portion provides three salt bridges in Mg^{2+} coordination *via* the α-, β- and γ-phosphates and remains identical in the PII^{OGex}, PII^{I86N} and $PII^{I86N\text{-}CIT}$ structures (see Figs. 4*a*–4*c*). The second sphere of coordination is formed in the wild-type PII^{OGex} structure by the oxo groups of 2-OG and Gln39, while citrate contributes three oxo groups for ligation. Another significant difference is the involvement

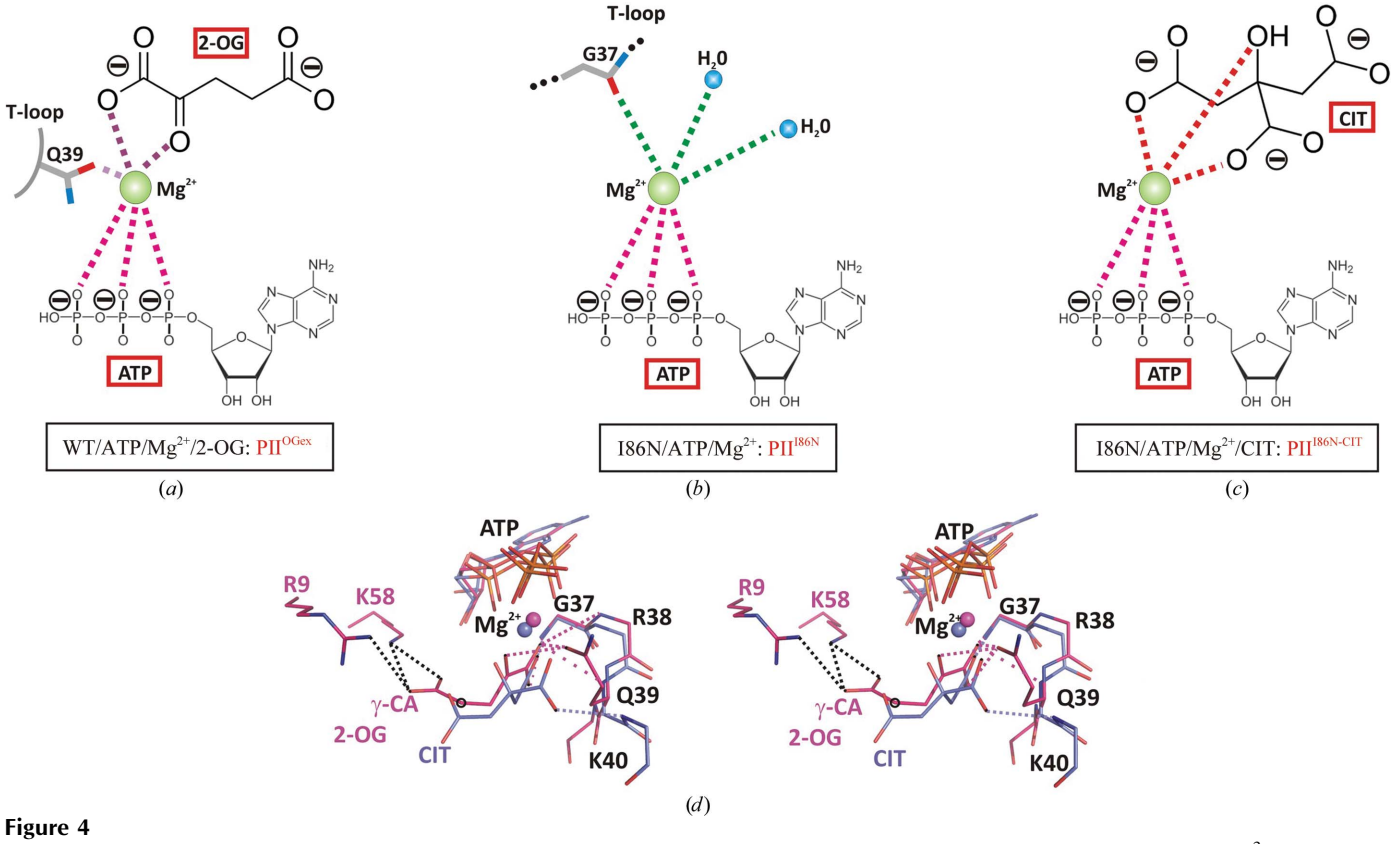

Figure 4
Plasticity of the chemical environment of magnesium in the 2-OG-bound and citrate-bound structures. (*a*) Hexagonal environment of Mg^{2+} in the 2-OG-bound structure (PDB entry 2xul) provided by the three phosphate groups of ATP, the carboxylate and carbonyl groups of 2-OG and the Gln39 side chain of the PII protein. (*b*) Coordination sphere of Mg^{2+} in $PII^{I86N\text{-}CIT}$, with ATP coordinating in the same way as in (*a*) to the backbone carbonyl group of Gly37 and two water molecules. (*c*) The coordination sphere of (*b*) is remodelled by the addition of citrate, which ligates the Mg^{2+} ion without additional factors *via* two carboxylate groups and the hydroxyl group. (*d*) Stereo figure and comparison between the active-site residues of the I86N mutant (blue) and the structure of wild-type PII in complex with ATP, Mg^{2+} and 2-OG (magenta). Interactions between the ligands and the surrounding residues are indicated by dashed lines. The methylene group which allows 2-OG to make interactions with the protein is shown in black. This group is missing in the citrate structure but is present in homocitrate.

of the conserved Lys58 residue, which forms a salt bridge to 2-OG, an interaction which was considered to be essential (Fokina, Chellamuthu, Forchhammer *et al.*, 2010; Truan *et al.*, 2010). This salt bridge is not formed with citrate and the lack of this interaction could explain why citrate but not 2-OG is able to approach the binding site in the PII-I86N variant closed by the Lys58–Glu44 salt bridge. The structure of the PII-I86N–citrate complex suggests that homocitrate would fit perfectly into the binding pocket of this PII variant. This idea resulted from analysis of a superposition of the structures containing 2-OG and citrate (see Fig. 4*d*). In the 2-OG structure the γ-carboxylate group forms two hydrogen bonds to residues Arg9 and Lys58. Although one carboxylate of the citrate ligand points towards these residues, the distance between the ligand and the protein is too long for a hydrogen bond. However, the introduction of an additional methylene group would allow the ligand to form the same hydrogen bonds to residues Arg9 and Lys58 and strengthen the overall binding constants. As shown below, homocitrate indeed affects PII-I86N function more efficiently than citrate (Fig. 5*c*).

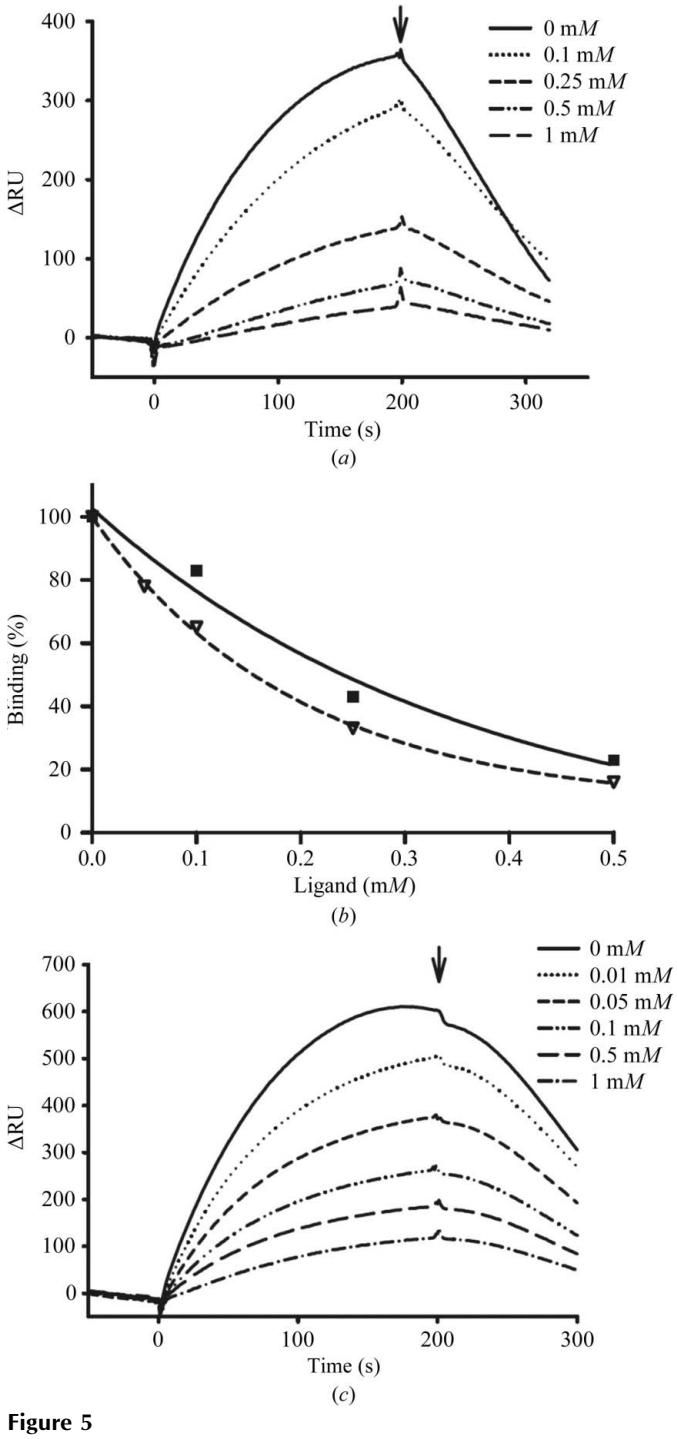

Figure 5
(*a*) SPR analysis of PII-I86N binding to R233A NAGK in the presence of 1 m*M* ATP and citrate at concentrations of 0, 0.1, 0.25, 0.5 and 1 m*M*. The response difference (ΔRU) between FC1 and FC2 is shown. An arrow indicates the end of the injection phase. (*b*) Association of PII-I86N and R233A NAGK in presence of citrate and 1 m*M* ATP (unbroken line) compared with wild-type PII and wild-type NAGK in the presence of 2-OG and 1 m*M* ATP (dashed line). (*c*) SPR analysis of PII-I86N binding to R233A NAGK in the presence of 1 m*M* ATP and homocitrate at concentrations of 0, 0.01, 0.05, 0.1, 0.5 and 1 m*M*.

3.3. Citrate is a second inhibitor of PII–NAGK interactions

To reveal whether citrate functionally replaces 2-OG in the I86N variant, the effect of citrate on the binding of PII-I86N to NAGK was assayed by SPR spectroscopy. Binding assays with wild-type NAGK showed no inhibitory effect of citrate (not shown); however, binding assays with the R233A NAGK variant showed a clear inhibitory effect of citrate (Fig. 5*a*). This resembles the inhibition of wild-type PII–NAGK association by 2-OG (Fig. 5*b*) and confirms that the citrate structure observed *in vitro* is indeed a functional metabolite signalling state. To test the prediction that homocitrate is an efficient ligand of PII-I86N, the inhibitory effect of this compound on PII–NAGK complex formation was tested by SPR analysis using surface-immobilized R233A NAGK (Fig. 5*c*). Homocitrate was more efficient than citrate in antagonizing the PII–NAGK interaction. Comparing the effects of both metabolites, 10 μ*M* homocitrate was as efficient as 100 μ*M* citrate. At a concentration of 1 m*M* both effectors were almost completely inhibitory for complex formation.

Why is citrate unable to disturb the interaction between PII-I86N and wild-type NAGK, while it affects the interaction of PII-I86N with the R233A variant of NAGK? Arg322 forms a salt bridge with Glu85 of PII which favours the bent T-loop conformation that fits into the NAGK crevice (Fokina, Chellamuthu, Zeth *et al.*, 2010). Presumably, this conformation reduces the stability of the citrate complex. However, without this salt bridge the citrate complex of PII-I86N is more stable than the PII-I86N–R233A NAGK complex. From this result, it follows that citrate binding to the PII-I86N variant is weaker than 2-OG binding to wild-type PII.

Based on the findings in this study, PII proteins could now be designed that allow the measurement of different metabolites. The I86N variant in complex with citrate is the first example of a genetically engineered PII protein that senses a novel metabolite.

The authors are grateful for the financial support provided by the Max Planck Society and the University of Tübingen, Germany and to the German Science Foundation (DFG) for the grant to KF (FO195/9-1). We cordially thank Reinhard Albrecht and Vasuki Ranjani-Chellamuthu for their help in crystallization of the mutant protein and crystal handling. The authors wish to thank the entire beamline staff of PXII at the Swiss Light Source (SLS) for beamline maintenance and continuous support.

References

Bueno, R., Pahel, G. & Magasanik, B. (1985). *J. Bacteriol.* **164**, 816–822.
Burillo, S., Luque, I., Fuentes, I. & Contreras, A. (2004). *J. Bacteriol.* **186**, 3346–3354.
Cheah, E., Carr, P. D., Suffolk, P. M., Vasudevan, S. G., Dixon, N. E. & Ollis, D. L. (1994). *Structure*, **2**, 981–990.
Emsley, P. & Cowtan, K. (2004). *Acta Cryst.* D**60**, 2126–2132.
Espinosa, J., Forchhammer, K., Burillo, S. & Contreras, A. (2006). *Mol. Microbiol.* **61**, 457–469.
Espinosa, J., Forchhammer, K. & Contreras, A. (2007). *Microbiology*, **153**, 711–718.
Fokina, O., Chellamuthu, V. R., Forchhammer, K. & Zeth, K. (2010). *Proc. Natl Acad. Sci. USA*, **107**, 19760–19765.
Fokina, O., Chellamuthu, V. R., Zeth, K. & Forchhammer, K. (2010). *J. Mol. Biol.* **399**, 410–421.
Fokina, O., Herrmann, C. & Forchhammer, K. (2011). *Biochem. J.* **440**, 147–156.
Forchhammer, K. (2008). *Trends Microbiol.* **16**, 65–72.
Forchhammer, K. & Hedler, A. (1997). *Eur. J. Biochem.* **244**, 869–875.
Heinrich, A., Maheswaran, M., Ruppert, U. & Forchhammer, K. (2004). *Mol. Microbiol.* **52**, 1303–1314.
Jiang, P. & Ninfa, A. J. (2007). *Biochemistry*, **46**, 12979–12996.
Kabsch, W. (2010). *Acta Cryst.* D**66**, 125–132.
Laskowski, R. A., MacArthur, M. W., Moss, D. S. & Thornton, J. M. (1993). *J. Appl. Cryst.* **26**, 283–291.
Leigh, J. A. & Dodsworth, J. A. (2007). *Annu. Rev. Microbiol.* **61**, 349–377.
Llácer, J. L., Contreras, A., Forchhammer, K., Marco-Marín, C., Gil-Ortiz, F., Maldonado, R., Fita, I. & Rubio, V. (2007). *Proc. Natl Acad. Sci. USA*, **104**, 17644–17649.
Llácer, J. L., Espinosa, J., Castells, M. A., Contreras, A., Forchhammer, K. & Rubio, V. (2010). *Proc. Natl Acad. Sci. USA*, **107**, 15397–15402.
Maheswaran, M., Urbanke, C. & Forchhammer, K. (2004). *J. Biol. Chem.* **279**, 55202–55210.
Maier, S., Schleberger, P., Lu, W., Wacker, T., Pfluger, T., Litz, C. & Andrade, S. L. (2011). *PLoS One*, **6**, e26327.
Mizuno, Y., Berenger, B., Moorhead, G. B. & Ng, K. K. (2007). *Biochemistry*, **46**, 1477–1483.
Murshudov, G. N., Skubák, P., Lebedev, A. A., Pannu, N. S., Steiner, R. A., Nicholls, R. A., Winn, M. D., Long, F. & Vagin, A. A. (2011). *Acta Cryst.* D**67**, 355–367.
Ninfa, A. J. & Jiang, P. (2005). *Curr. Opin. Microbiol.* **8**, 168–173.
Sakai, H., Wang, H., Takemoto-Hori, C., Kaminishi, T., Yamaguchi, H., Kamewari, Y., Terada, T., Kuramitsu, S., Shirouzu, M. & Yokoyama, S. (2005). *J. Struct. Biol.* **149**, 99–110.
Sant'Anna, F. H., Trentini, D. B., de Souto Weber, S., Cecagno, R., da Silva, S. C. & Schrank, I. S. (2009). *J. Mol. Evol.* **68**, 322–336.
Studier, F. W., Rosenberg, A. H., Dunn, J. J. & Dubendorff, J. W. (1990). *Methods Enzymol.* **185**, 60–89.
Truan, D., Huergo, L. F., Chubatsu, L. S., Merrick, M., Li, X.-D. & Winkler, F. K. (2010). *J. Mol. Biol.* **400**, 531–539.
Vagin, A. & Teplyakov, A. (2010). *Acta Cryst.* D**66**, 22–25.
Xu, Y., Carr, P. D., Clancy, P., Garcia-Dominguez, M., Forchhammer, K., Florencio, F., Tandeau de Marsac, N., Vasudevan, S. G. & Ollis, D. L. (2003). *Acta Cryst.* D**59**, 2183–2190.
Xu, Y., Carr, P. D., Huber, T., Vasudevan, S. G. & Ollis, D. L. (2001). *Eur. J. Biochem.* **268**, 2028–2037.
Xu, Y., Cheah, E., Carr, P. D., van Heeswijk, W. C., Westerhoff, H. V., Vasudevan, S. G. & Ollis, D. L. (1998). *J. Mol. Biol.* **282**, 149–165.
Yidiz, Ö., Kalthoff, C., Raunser, S. & Kühlbrandt, W. (2007). *EMBO J.* **26**, 589–599.